Molecular Cell
Article

Mechanism of Gate Opening in the 20S Proteasome by the Proteasomal ATPases

Julius Rabl,[1,2,5,6] David M. Smith,[2,5] Yadong Yu,[3] Shih-Chung Chang,[4] Alfred L. Goldberg,[2] and Yifan Cheng[3,*]
[1]Fachbereich Biologie, Chemie, Pharmazie, Freie Universität Berlin, Takustrasse 3, 14195 Berlin, Germany
[2]Department of Cell Biology, Harvard Medical School, 240 Longwood Avenue, Boston, MA 02115, USA
[3]The W.M. Keck Advanced Microscopy Laboratory, Department of Biochemistry and Biophysics, University of California, San Francisco, 600 16th Street, San Francisco, CA 94158, USA
[4]Institute of Microbiology and Biochemistry, National Taiwan University, 1 Roosevelt Road, Taipei, 10617 Taiwan
[5]These authors contributed equally to this work.
[6]Present address: Institute of Molecular Biology and Biophysics, ETH Zurich, 8093 Zurich, Switzerland.
*Correspondence: ycheng@biochem.ucsf.edu
DOI 10.1016/j.molcel.2008.03.004

SUMMARY

Substrates enter the cylindrical 20S proteasome through a gated channel that is regulated by the ATPases in the 19S regulatory particle in eukaryotes or the homologous PAN ATPase complex in archaea. These ATPases contain a conserved C-terminal hydrophobic-tyrosine-X (HbYX) motif that triggers gate opening upon ATP binding. Using cryo-electron microscopy, we identified the sites in the archaeal 20S where PAN's C-terminal residues bind and determined the structures of the gate in its closed and open forms. Peptides containing the HbYX motif bind to 20S in the pockets between neighboring α subunits where they interact with conserved residues required for gate opening. This interaction induces a rotation in the α subunits and displacement of a reverse-turn loop that stabilizes the open-gate conformation. This mechanism differs from that of PA26/28, which lacks the HbYX motif and does not cause α subunit rotation. These findings demonstrated how the ATPases' C termini function to facilitate substrate entry.

INTRODUCTION

The majority of the protein degradation in eukaryotic cells is catalyzed by the 26S proteasome, an ATP-dependent proteolytic complex (Goldberg, 2005). It is composed of the 20S core proteasome and two 19S regulatory complexes that bind the ubiquitinated substrates, unfold them, and translocate them into the 20S, where they are hydrolyzed to small peptides (Coux et al., 1996; Voges et al., 1999). The 20S particle is a hollow barrel-shaped structure composed of four stacked heptameric rings. Its two inner β rings and two outer α rings form three continuous internal chambers (Groll et al., 1997; Lowe et al., 1995), and its multiple proteolytic active sites are sequestered in the central chamber (Seemuller et al., 1995). Protein substrates enter the 20S through a gated pore in the center of the α ring. The N-terminal tails of the α subunits form the gate (Groll et al., 1997, 2000). A key role of the six ATPases in the 19S particle is to open this gate and thus to facilitate substrate entry (Kohler et al., 2001; Smith et al., 2005). Archaea contain a homologous but simpler 20S proteasome, whose activation is regulated similarly by the ATPase complex called PAN (Benaroudj and Goldberg, 2000; Benaroudj et al., 2003; Smith et al., 2005). PAN is a hexameric ring complex that is homologous to the ATPase ring in the base of the 19S particle, but it offers many advantages for mechanistic studies. Upon binding of ATP, PAN associates with the α rings of the 20S and induces gate opening, which allows peptides and unfolded proteins to diffuse into the 20S's internal chamber and be degraded (Smith et al., 2005).

We recently showed (Smith et al., 2007) that PAN from *Methanococcus jannaschii* and three of the six eukaryotic 26S ATPases contain a conserved three-residue C-terminal motif: hydrophobic-tyrosine-X (HbYX), which is essential for ATP-dependent gate opening and for the association of PAN with the 20S particle. Upon binding of ATP or a nonhydrolyzable ATP analog to PAN, its C termini associate with sites on the 20S's α ring and trigger gate opening. Furthermore, peptides of seven residues or longer that correspond to PAN's C-terminal sequence can by themselves cause gate opening and compete with PAN for binding to the archaeal 20S. Thus, these short peptides and PAN bind to the same sites and cause gate opening by the same mechanism.

Most likely, these C-terminal residues interact with pockets between the α subunits because a mutation in these pockets (K66A) prevents PAN-20S association and gate opening (Smith et al., 2007). This HbYX-dependent mechanism is conserved in eukaryotic proteasome, because peptides from PAN's C terminus induce gate opening in the mammalian 20S as do C-terminal peptides from two of the 19S ATPase subunits, Rpt2 and Rpt5, which contain the HbYX motif. Moreover, mutating these terminal residues in each of the individual 19S ATPases in yeast also affects gating and reduces the stability of the 26S complex.

Much has been learned about the mechanism of gate opening in the 20S by a very different type of proteasome activator, PA26, from *Trypanosoma brucei*. This heptameric 11S complex is a homolog of the mammalian PA28αβ (REG) complex, which enhances antigen presentation (Dubiel et al., 1992; Knowlton et al., 1997; Ma et al., 1992), and the nuclear PA28γ complex, which can stimulate degradation of some nuclear proteins

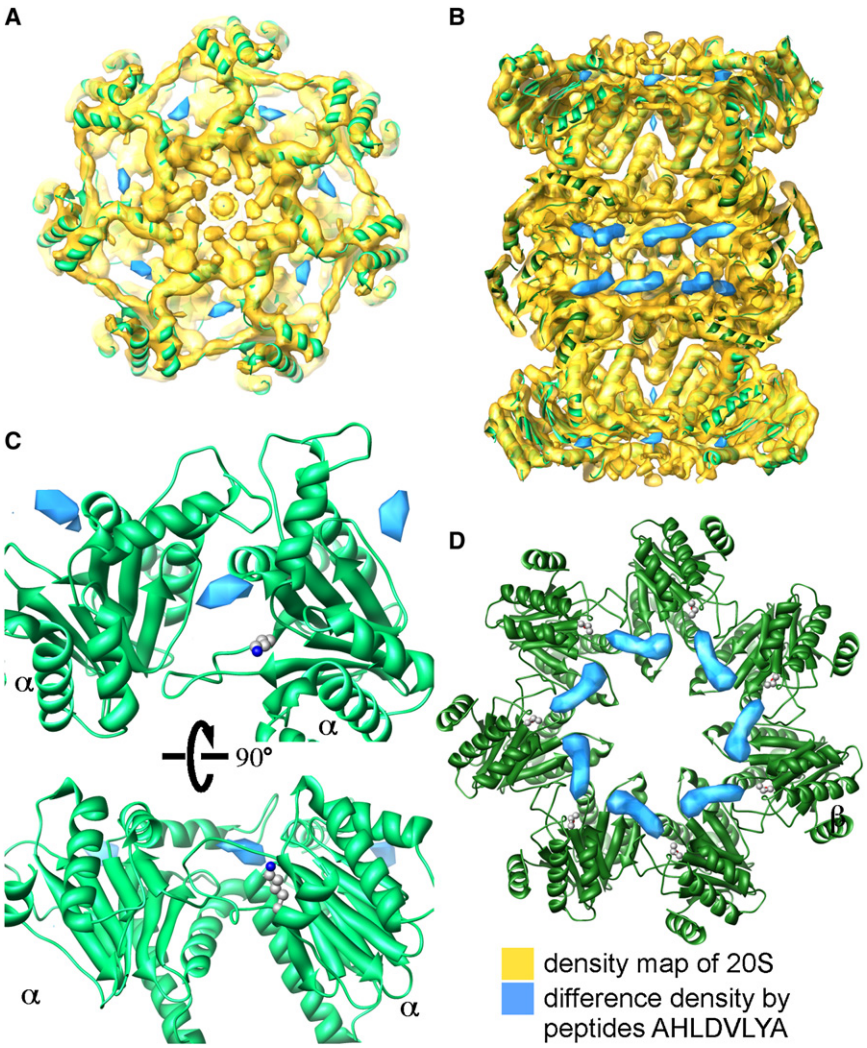

Figure 1. Difference Map Reveals the Binding Sites of the Peptides to 20S

(A and B) Top and side (cut in half and looking from inside out) views of 3D density map of 20S (yellow) with the atomic structure (PDB code, 1PMA; green ribbon diagram) docked. Superimposed are difference densities (blue, 6σ, where σ is rmsd from mean) between the 20S-AHLDVLYA and the 20S.

(C) Top and side views of two adjacent α subunits (light green) with the difference densities that indicate the binding sites of the peptides. The side chain of Lys66 is shown.

(D) Structure of the β ring (dark green) superimposed with the difference densities that correspond to peptides bound to the proteolytic sites. The side chains of the active-site Thr1 are shown.

(Masson et al., 2001). These heptameric complexes also associate with the proteasome's α rings, but their precise effects on proteasomal function remain unclear. Their C termini are not conserved and lack the HbYX motif or any other homology to the ATPases' C termini. Nevertheless, the crystal structures of the yeast and archaeal 20S complexed with PA26 (Forster et al., 2003, 2005; Whitby et al., 2000) showed that when PA26 binds to the 20S α ring, its C termini insert into the seven intersubunit pockets found between two adjacent α subunits. However, to induce gate opening, PA26 requires also an "activation loop" (Zhang et al., 1998) to move a reverse turn in the α subunits to stabilize the open conformation. The proteasomal ATPases, however, must use a very different mechanism to induce gate opening because short peptides containing their C-terminal sequence can by themselves induce gate opening, while those from PA26 cannot do so (Smith et al., 2007).

The present studies were undertaken to define the structural basis and mechanism of gate opening induced by the regulatory ATPases' C termini. Using single particle cryo-electron microscopy (cryo-EM), we have localized the specific binding sites of the ATPases' C termini in the 20S from *Thermoplasma acidophilum*. We have also determined the structures of the 20S's closed and open gate, as well as the associated conformational changes in the α subunits that are induced by these peptides to cause gate opening.

RESULTS

Cryo-EM of 20S Complexed with Synthetic Peptides

To clarify the mechanism by which the proteasomal ATPases' C termini open the 20S gate to facilitate substrate entry, we attempted to visualize how the C termini of PAN bind to the 20S and induce gate opening. We used synthetic peptides of seven or eight residues that mimic PAN's C termini (Seong et al., 2002; Smith et al., 2007) and determined by single particle cryo-EM the structures of the frozen hydrated *T. acidophilum* 20S alone and with four different peptides that can or cannot cause gate opening (see Figure S1 available online). The seven-residue peptide HLDVLYR corresponds to the C terminus of PAN (from *Methanococcus jannaschii*), contains the conserved HbYX motif, and induces gate opening in the 20S (Smith et al., 2007). The eight-residue peptide AHLDVLYA differs in having an alanine in place of the C-terminal arginine, but this change does not alter its ability to cause gate opening (Smith et al., 2007). The related peptide AHLDVLAR contains an alanine in place of the conserved tyrosine, which disrupts the HbYX motif and abrogates its gate-opening ability (Smith et al., 2007). The fourth peptide, GTDHMVS, corresponds to the C terminus of PA26, which lacks the conserved HbYX motif and therefore cannot, by itself, induce gate opening (Smith et al., 2007).

For each of the specimens, we selected more than 40,000 particles of frozen hydrated 20S from digitized electron micrographs (Figure S1A). Three-dimensional (3D) reconstructions with D7 symmetry were calculated from the 20S by itself (at a nominal resolution of 6.8 Å, using FSC = 0.143 criterion) and after incubation with the peptides HLDVLYR (7.5 Å), AHLDVLYA (5.6 Å),

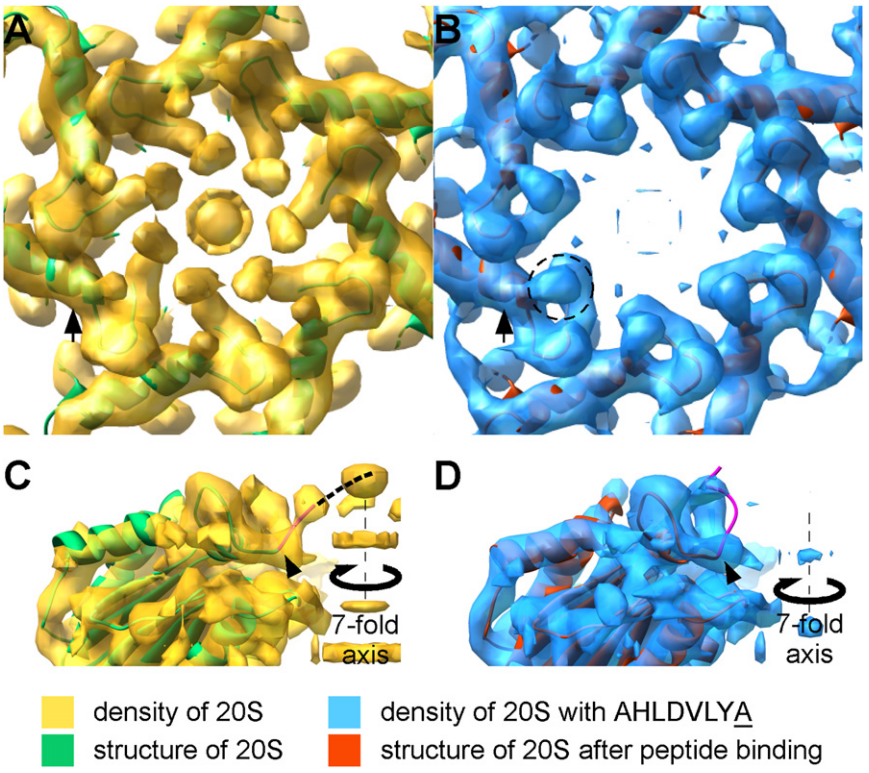

Figure 2. The Closed and the Open Gate of 20S

(A and B) Density maps of the closed gate ([A], yellow) and the open gate ([B], blue), with the structure of the docked α subunits (ribbon diagram).

(C and D) Densities of an individual α subunit boxed out from (A) and (B). The symmetry axes are marked. Beyond Thr13 (identified by arrowheads), the structures are modeled (magenta) to fit the densities of both the closed- and open-gate conformations. The dashed line in (C) marked a possible way the remaining residues in the N terminus may extend further into the pore.

AHLDVLAR (8.1 Å), and GTDHMVS (6.1 Å) (Figure S1B). Most particles selected were side views of the 20S (Figure S1C), which corresponded to the orientations of most of the barrel-shaped 20S embedded in the vitreous ice (Figure S1D). These nominal resolutions of our 3D reconstructions were confirmed by comparing them with the density maps calculated from the atomic structure and filtered to the same resolutions (Figure S2).

Figures 1A and 1B show the excellent agreement between the 20S density map determined by cryo-EM (shown in yellow) and the docked atomic structure of the 20S from *T. acidophilum* (shown in green) determined by X-ray crystallography (PDB code, 1PMA [Lowe et al., 1995]). All the α helices are clearly resolved in the density maps, as are the β sheets sandwiched between the α helices. To determine the locations where peptides bind to the 20S, we calculated the difference maps by subtracting the density of the 20S from the densities of the 20S with the peptides.

The peptide-induced difference densities by either of the gate-opening peptides, AHLDVLYA (shown in blue in Figure 1) and HLDVLYR (shown in red in Figure S3), appeared in two locations: on the outer surface of the α rings (Figure 1A and Figure S3A) and within the particles' central chamber on each of the β rings (Figure 1B and Figure S3B). On the outer ring, there were seven identical sites where the peptides from the C termini of PAN bound in the pockets between the adjacent α subunits (Figure 1C and Figure S3C). Located in these pockets is Lys66, which was shown to be essential for gate opening by PAN and the HbYX peptides (Smith et al., 2007). Consequently, this pocket was suggested to be the likely site for binding of the C termini of PAN (Smith et al., 2007), and it is also where the C terminus of PA26 binds (Forster et al., 2005).

The archaeal 20S contains 14 identical proteolytic sites located at the N termini of the seven β subunits. In the absence of PAN and ATP, the gate in the α ring is closed and excludes seven-residue or larger peptides (Smith et al., 2005). However, binding of the peptides from PAN's C terminus by itself induces gate opening, which allows peptides to diffuse into the 20S's central chamber, where they can bind to the active sites (Figure 1D and Figure S3D). Accordingly, we found difference densities within the 20S central chamber that correspond to these peptides associated with the seven active sites.

When the related peptides that are unable to cause gate opening were present, i.e., AHLDVLAR (a variant of PAN's C terminus lacking the HbYX motif) and GTDHMVS (from PA26's C terminus) (Smith et al., 2007), some difference densities were also found in the intersubunit pockets but these densities were much weaker than those generated by the gate-opening HbYX-motif peptides (Figure S4A). These densities were also located in a different region than the gate-opening peptides, close to the helix H0, but above the pocket (Figure S4C), and they may correspond to the weak association of these non-gate-opening peptides with the 20S, observed previously (Smith et al., 2007). Nevertheless, with these peptides, no densities were observed in the active sites within the central chamber (Figure S4B), presumably because they failed to open the gate (see below) and were thus excluded from the particle, even though they were present at a very high concentration (1 mM).

Structures of the Closed and Open Gate in the 20S

When gently isolated, the proteolytic activity of the 20S is latent (Coux et al., 1996), and the crystal structure of the yeast 20S shows a closed gate that prevents the entry of substrates (Groll et al., 1997, 2000). In contrast, in the crystal structure of the 20S from archaea, *T. acidophilum*, the first 12 N-terminal residues of the seven α subunits appeared to be disordered, and it was initially interpreted to mean that substrates had an unimpeded path of entry into the 20S through the central pore (Lowe et al., 1995). However, subsequent biochemical and mutational studies showed that the archaeal (like the eukaryotic) 20S does have a functioning gate that is formed by the N termini of the α subunits

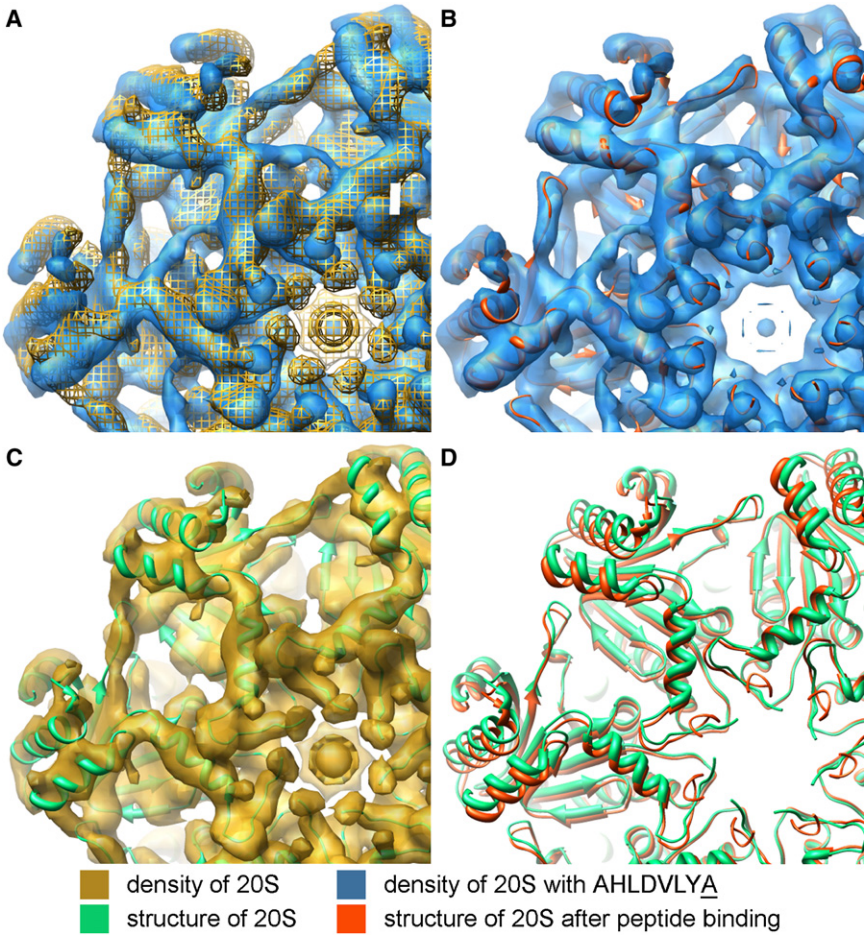

Figure 3. Conformational Change of 20S α Ring Induced by the Gate-Opening Peptides

(A) Top view of superimposed density maps of 20S (gold mesh) and 20S-AHLDVLYA complex (blue transparent surface).

(B) Top view of the 20S-AHLDVLYA density map (blue) with the structure of the open-gate 20S docked.

(C) Top view of the 20S density map (gold) with the structure of the closed-gate 20S docked.

(D) Superimposed structures of 20S with the open and the closed gate.

(Benaroudj et al., 2003; Smith et al., 2005, 2007). Accordingly, the density map of the 20S shows within the central pore densities corresponding to the N termini of the α subunits. Moreover, these densities extended beyond the last residue identified in the atomic structure, Thr13 (Lowe et al., 1995), and project toward the center of the pore in the α ring (Figure 2A), restricting substrate entry.

The diameter of the closed gate was 9 Å when measured directly from the density map (at the density level of 2σ). This is much smaller than the diameter of the central channel of about 23 Å as defined by Thr13, the first resolved residue in the crystal structure. Importantly, the diameter of the closed gate visualized by our cryo-EM density map is much smaller than the 13 Å diameter of the α-annulus, through which substrates enter the central chamber. We have extended the atomic structure of the N termini of the α subunits from Thr13 to Arg10 by positioning its main chain in the density that forms the gate (Figure 2C). Therefore, the structure of the closed gate of the archaeal 20S clearly is more ordered than previously thought. The first nine residues of the α subunits' N termini are still missing in the density map (at 2σ), probably because they are more disordered than residues beyond Arg10, which are very close to the center of the pore. The remaining disordered N-terminal residues from all seven α subunits are likely to extend further into the pore, blocking the free passage of oligopeptides larger than seven residues (Smith et al., 2005). The density located in the center of the pore (Figures 2A and 2C), which we see in all of our reconstructions of the closed-gate form, probably corresponds to these extended N termini of the α subunits (hatched line in Figure 2C).

The density map of the 20S with the gate-opening peptide, AHLDVLYA, bound showed a very different structure of the central pore (Figure 2B). In contrast to the closed conformation, this "open" form showed no density extending into the center of the pore to block substrate entry into the 20S. Instead, there was an additional density (marked by a dashed circle in Figure 2B) attached to the α subunit, outside of the pore. In this form, the pore has a diameter of about 20 Å, which is much larger than the pore size in the closed conformation (9 Å). We extended the atomic structure of the N termini from Thr13 to Ala7 by fitting the densities observed in the open-gate conformation (Figure 2D). In this model, Ala7 is located away from the pore with the N termini projecting up and away from the 7-fold axis. In contrast, the density map of the 20S with the seven-residue C-terminal peptide from PA26, GTDHMVS, or the inactive variant, AHDVLAR, both of which do not induce gate opening (Smith et al., 2007), showed no change in the conformation of the α subunits. Also, the gating residues remained in the same positions as in the closed form (data not shown).

Conformational Changes in the α Ring Associated with Gate Opening

The binding of the C-terminal peptides to the intersubunit pockets also caused a conformational change in the α subunits that appears to trigger gate opening. We compared the three density maps with the highest resolutions, that of the 20S alone, the 20S with AHLDVLYA, and the 20S with GTDHMVS. These density maps were filtered to the same resolution, 6.8 Å, to facilitate comparisons and to visualize this conformational change. The densities of the maps of the 20S by itself and in complex with the AHLDVLYA overlap very well in two central β rings,

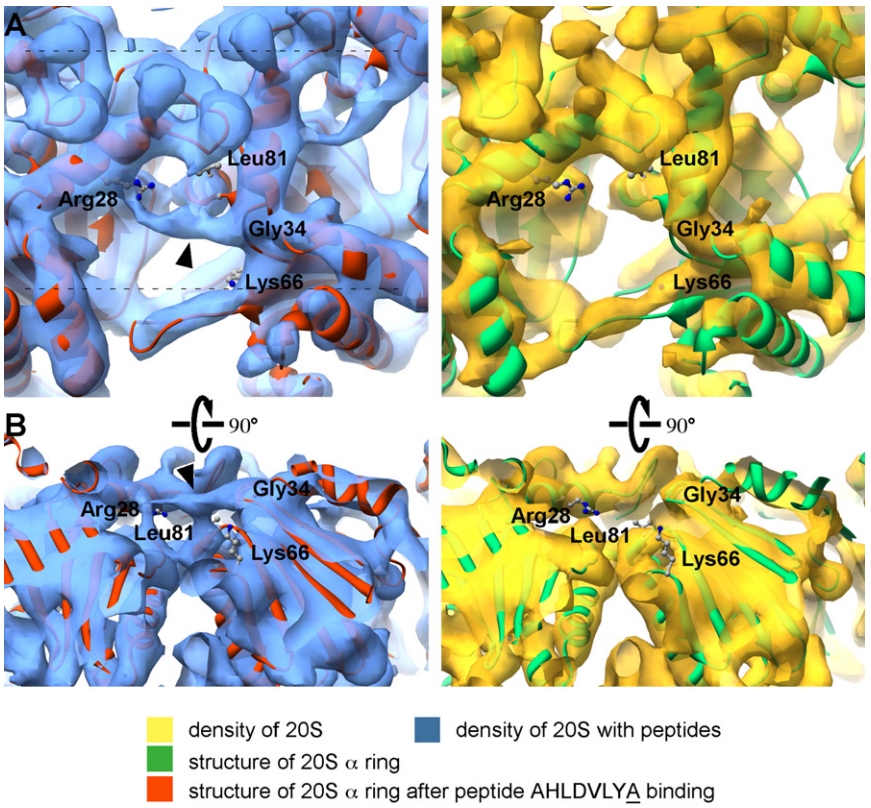

Figure 4. Interactions of the Gate-Opening Peptides with the 20S

(A) Top view of the pocket between adjacent α subunits with (left) and without (right) peptide bound. (B) Side view of the same pocket (90° rotated) and the density slab within the dashed line in (A) with (left) and without (right) peptide bound. Residues that may be involved in peptide binding are marked. Notice that the density identified by the arrowhead (left) is not present in the density map without the bound peptide (right).

but they differed in the outer α rings (Figure 3A and Figures S5A and S5B). Therefore, the binding of the gate-opening peptide induced a conformational change in the α ring.

We docked the atomic structure of the entire *T. acidophilum* 20S (Lowe et al., 1995) into the density map of 20S-AHLDVLYA by refining the fitting of the β ring only. While the atomic structure of the entire β ring fit very well into the density map, the α ring did not (Figure S5C, left). A good fit of the atomic structure into the cryo-EM density of the α ring was achieved only when the docking of the individual α subunits was refined as rigid bodies (Figure 3B and Figure S5C, right). Comparison of the structures of the α subunits before (Figure 3C) and after binding (Figure 3B) of the gate-opening peptide revealed that each 20S α subunit undergoes a rotation pivoting around Gly128 (Figure 3D) (Cα atom moved 0.4 ± 0.1 Å). Gly128 is a key residue in a highly conserved loop (Tyr126-Gly127-Gly128), which, together with the corresponding loops from six other α subunits, forms the α-annulus at the entrance of the outer chamber. Thus, upon binding of the gate-opening peptides, each α subunit rotates around this α-annulus by about 4°.

No such conformational change was observed in the crystal structure of the archaeal 20S complexed with PA26 (Forster et al., 2005), nor in our density map of the 20S with the PA26's C-terminal peptide GTDHMVS, which does not trigger gate opening (Smith et al., 2007) (Figure S6). In addition, the mechanism, as well as the pivot point of the rotation induced by the ATPases' C termini, differs from the conformational change in the archaeal and the eukaryotic 20S α subunits, when complexed with PA26 (Forster et al., 2003).

Binding Sites for the Gate-Opening Peptide

The binding of both PAN and peptides from PAN's C terminus that triggers gate opening requires the conserved C-terminal HbYX motif, which must interact with specific residues in the intersubunit pockets. Figures 4A and 4B compare the structures of these pockets with (left) and without (right) a bound gate-opening peptide. Despite its small size, the density corresponding to the bound peptide, AHLDVLYA, was clearly visible spanning across the pocket and interacting with the two adjacent α subunits. The peptide was located above Lys66, which is required for gate opening by the C termini of PAN as well as PA26 (Forster et al., 2005; Smith et al., 2007), but no density connecting this peptide to Lys66 was evident at this resolution. However, a strong density was found linking the peptide to Gly34 and to the hydrophobic residue, Leu81, of one α subunit, and a relatively weaker density connecting it to Arg28 of the adjacent α subunit. Thus, the conserved C-terminal HbYX motif appears to interact with Gly34 and Leu81, which are highly conserved in the archaeal 20S and in most of the α subunits of the eukaryotic 20S. The remaining four (or five) N-terminal residues of the peptide appear to span across the pocket and may interact with the neighboring α subunit near Arg28. To open the 20S gate, a C-terminal peptide must also be at least seven residues long (Smith et al., 2007), and as shown in Figures 4A and 4B, these gate-opening peptides seem to interact with both of the adjacent α subunits. Possibly, the gate-opening peptides need to be seven residues long in order to span the pocket.

Because of the apparent interaction of the peptides with Leu81 and its neighboring hydrophobic residue Val82, we tested the importance of these residues by mutation. Leu81 is a highly conserved hydrophobic residue in the α subunits of both archaeal and eukaryotic 20S, while Val82 is not (Table S1). We mutated the Leu81 and Val82 either separately or both together to an alanine or to the charged residues glutamic acid and aspartic acid, and tested whether three different activators could induce gate opening in these mutant 20S (measured by LFP hydrolysis [Smith et al., 2007]). Neither PAN (Figure 5A), its C-terminal peptides (Figure 5B), nor PA26 (Figure 5C) stimulated gate opening in

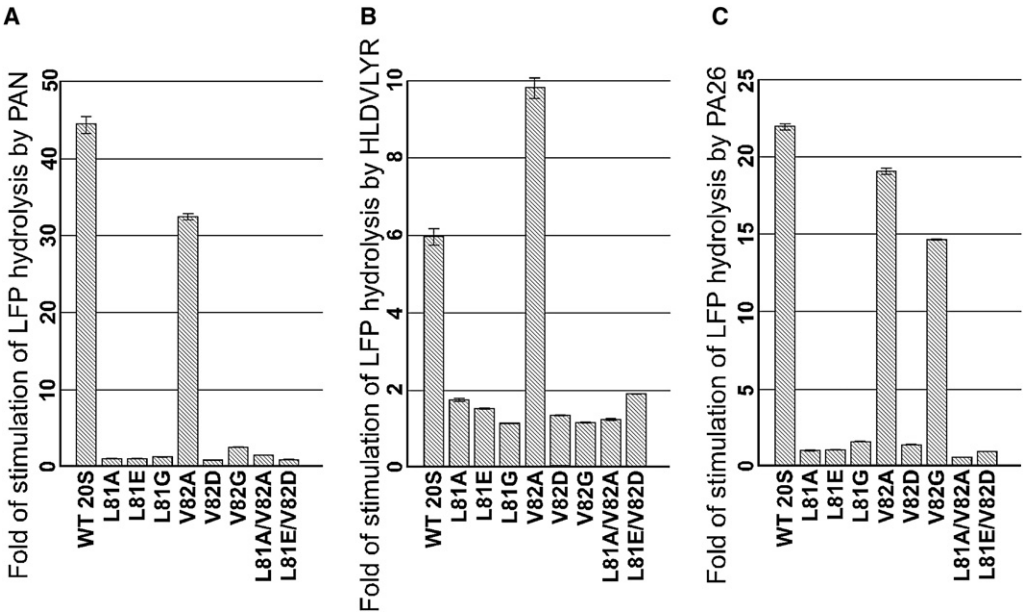

Figure 5. Abilities of Three Different Activators to Stimulate the Gate Opening of 20S Mutants

20S proteasome (0.2 μg of wild-type or various Leu81/Val82 mutants) and LFP are incubated with (A) PAN in a molar ratio of 10:1 of 20S, (B) 250 μM of peptide HLDVLYR, and (C) PA26 in a molar ratio of 30:1 of 20S. The stimulation of gate opening was measured by the increase of LFP hydrolysis over wild-type 20S without any activator. The values are means ± standard deviations from at least three independent experiments.

the single mutants of Leu81 or in any of the double mutants. In contrast, the replacement of Val82 by alanine did not affect the ability of these three different activators to stimulate gate opening, but mutation to a negatively charged aspartic acid did prevent gate opening by all these activators. Thus, the hydrophobic residue Leu81 (but not Val82) appears to be required for the interaction with the C termini of PAN as well as PA26. In addition, we mutated Val82 to glycine. In this mutant, neither PAN nor its C-terminal peptides could stimulate substrate entry, but surprisingly, PA26 still stimulates as well as in the wild-type 20S. We also observed by negative-staining EM that the 20S V82G mutant still forms a complex with PA26, but not with PAN (data not shown). This difference in activation of the V82G mutant provides further evidence that PAN and its C-terminal peptides interact with the same residues in the intersubunit pockets and function by the same mechanism, but that PA26 binds differently to the intersubunit pocket and causes gate opening by a distinct mechanism (see below).

The Mechanism of Gate Opening by the Proteasomal ATPases

The crystal structure of the PA26-20S complex (Forster et al., 2005) reveals that the activation loop of PA26 causes gate opening by inducing a radial and lateral displacement of a critical reverse-turn loop in the α subunits involving Pro17 (Figure 6B, right) (Forster et al., 2005). We show here that the binding of the ATPases' C-terminal peptides to the intersubunit pockets also induces gate opening by causing a displacement of this same reverse-turn loop, but it does so without an activation loop and without contacting Pro17. Instead, the rigid body rotation of the α subunits induced by binding of the HbYX-containing peptides from PAN results in this displacement. The measured 1.5 ± 0.1 Å displacement of Pro17 (Figure S5B, right) based on a rigid body rotation of the α subunits of ~4° after peptide binding reassembles closely the displacement induced by PA26's activation loop. The enlarged views of the α ring shown in Figure 6 demonstrate the similar changes in position of Pro17 before and after binding of the gate-opening peptides (Figure 6A, right) and before and after binding of PA26 (Figure 6B, right).

These observations suggest the following gate-opening mechanism induced by nucleotide binding to the proteasomal ATPases: upon association of PAN with the 20S, the HbYX motif of PAN's C termini binds to specific residues (e.g., Gly34, Lys66, and Leu81) in the intersubunit pockets. This binding causes a rotation of the individual α subunits, resulting in the radial and lateral movement of the Pro17 away from the pore, which stabilizes the open-gate conformation. This open conformation appears to be the same as that induced by PA26/28 family of proteasome activators. Thus, the binding of PAN's C terminus by itself triggers movement of the Pro17 residue in the α subunits to form a stable open-gate conformation.

DISCUSSION

These and our prior studies demonstrate a mechanism of proteasomal ATPases' induced gate opening in the 20S, which is conserved from archaeal to mammalian 26S proteasome (Smith et al., 2007). To our surprise, this ATP-dependent mechanism involves the same relocation of the Pro17 loop as PA26 causes, although this movement is achieved through a very different mechanism. Hill and coworkers (Forster et al., 2003, 2005) previously showed that PA26's activation loop stabilizes the open

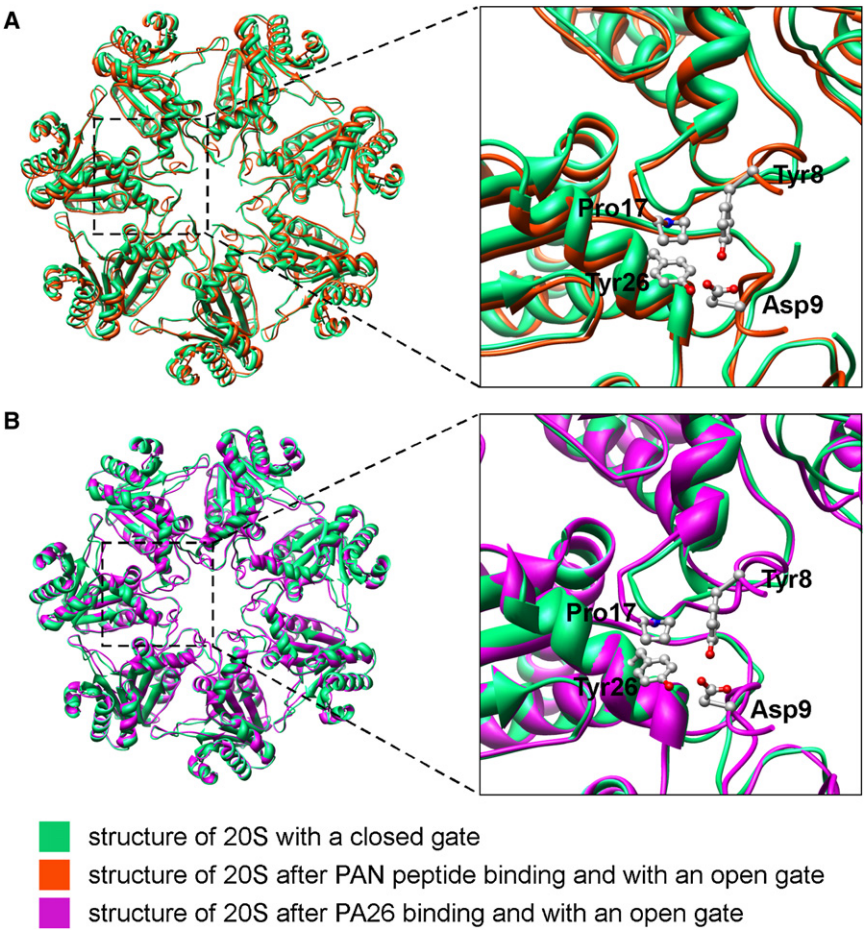

Figure 6. Mechanism of Gate Opening in the 20S Induced by PAN and PA26 Complexes

(A) (Left) Overlay of the α ring structures, before and after the binding of the gate-opening peptides. (Right) Enlarged view of the dashed area from the left. Pro17 is shifted because of the rotation in α subunit.

(B) (Left) Overlay of the structure of the α ring, before and after PA26 binding. (Right) Enlarged view of the dashed area. Pro17 is shifted by the activation loop of PA26 (data not shown). Notice that Pro17 in red and magenta structures is in a similar position.

conformation by directly interacting with this loop. The key difference in PA26's and PAN's gate-opening mechanism is in how each moves the Pro17 to stabilize the open conformation. Binding of PA26's seven C termini to the seven intersubunit pockets by itself does not induce this shift, which instead requires contact of the seven Pro17 residues with PA26's seven activation loops. By contrast, when PAN is in its ATP-bound conformation, the association of its C-terminal residues with these same pockets by themselves causes a rotation of the entire α subunit, resulting in a very similar Pro17 shift. Therefore, while each PA26 subunit requires two interactions with the 20S for gate opening (involving its C terminus and the activation loop), PAN requires only one, its C terminus. However, the open-gate conformation of the gating residues induced by these two very different regulators appears to be identical.

These distinct mechanisms must reflect differences in the C-terminal sequences of PAN and PA26 and their interactions with the 20S. The crystal structure of the 20S-PA26 complex showed that PA26's C-terminal main chains form antiparallel β sheet-like hydrogen bonds with the residues in the intersubunit pockets (Forster et al., 2003). Thus, PA26 does not require a conserved sequence in its C terminus to activate the 20S (Forster et al., 2003; Whitby et al., 2000). The requirement for the conserved HbYX motif in PAN (and in the three 26S ATPases [Smith et al., 2007]) indicates that the formation of the PAN-20S complex and gate opening involve interactions of the C-terminal residues' side chains with the conserved residues in the 20S intersubunit pockets. Three of these 20S residues were identified (Gly34, Lys66, and Leu81), and the importance of Leu81 was confirmed here by mutagenesis. It is surprising that, although the C termini from both regulators bind to at least some of the same residues in these pockets, only the ATPases' C termini with the HbYX motif can by themselves cause a rotation of the α subunits to induce gate opening. In other words, the HbYX motif functions like a "key in a lock" to induce gate opening in the 20S proteasome.

These differences in the gate-opening mechanisms by PAN and PA26 appear to reflect their different biological roles and multimeric structures. To maintain the interaction between its activation loop and the reverse-turn loop in the α subunits, PA26 must be a rigid structure and form a stable complex with the 20S α ring. This association is probably favored because both the 20S α ring and PA26 are rigid, heptameric ring complexes that surround a central pore, through which substrates and peptide products pass. In contrast, there is a symmetry mismatch between the heptameric 20S α ring and the hexameric proteasomal ATPases. PAN and the 19S ATPases are members of the AAA ATPase family, which are all highly dynamic complexes that undergo transition and conformational change upon ATP hydrolysis (i.e., their gross structures differ in the ATP- and ADP-bound states [DeLaBarre and Brunger, 2005]). Perhaps the only possible mechanism for gate opening by such dynamic ATPase complexes is the transient docking of the C-terminal HbYX motif into some, but not all, of the intersubunit pockets. Although the present studies have focused on the completely open and completely closed conformations (e.g., Figures 2 and 6), it is likely that not all subunits bind the ATPases' C termini synchronously and that, at any instant, only some of the α subunits undergo this rotation and adopt the open-gate conformation. Such a gate-opening mechanism, involving only transient association of some of the six C termini with the 20S pockets, may be required by the proteasomal ATPases to undergo the ATP-driven conformational changes that catalyze the unfolding of

globular proteins and the translocation of polypeptides into the 20S, neither of which is catalyzed by the rigid PA26/28 complexes.

Although the eukaryotic 26S complex clearly evolved from the homologous archaeal 20S and PAN complexes, there are major structural differences: most importantly, the seven intersubunit pockets in the α ring differ from each other, as do the six 19S ATPases. Therefore, in addition to the symmetry mismatch problem discussed above, where all six ATPases' C termini clearly cannot bind simultaneously to the seven intersubunit pockets, in the 26S there are further structural restrictions on this HbYX mechanism. In the 19S, only four of the six ATPases contain the critical YX terminal residues, three of these contain the HbYX motif, and one contains a threonine in place of the Hb residue (Smith et al., 2007). Furthermore, octapeptides corresponding to the C termini of only two of the 19S ATPases, Rpt2 and Rpt5, both of which contain the HbYX motif, can by themselves induce gate opening in the eukaryotic 20S, in a similar manner as peptides from PAN's C termini (Smith et al., 2007). Nevertheless, each of these C-terminal YX residues is somehow involved in gating and/or 26S stability, though the different C termini play different roles (Smith et al., 2007).

In addition to these differences between the ATPases, the structures of the gate and each intersubunit pocket also differ in the eukaryotic 20S. Specifically, the N termini of only three of the seven α subunits (α2–α4) extend into the pore to form the closed gate, and the N terminus of α3 plays a special role in this structure. In addition, of the seven intersubunit pockets (Groll et al., 1997; Whitby et al., 2000), six contain the conserved Lys66 (or in one case, an arginine) (Table S1) that is essential for gate opening by the HbYX peptides and PAN. The other residue in the intersubunit pockets essential for gate opening, Leu81, is conserved as a hydrophobic residue in all α subunits. But the eukaryotic α2 has a glycine in the position of Val82 (Table S1). Based on the mutations in the archaeal 20S (Figure 5), it seems likely that the C termini of the critical ATPases Rpt2 and Rpt5 do not bind to the intersubunit pockets that lack a Lys66 or where there is a glycine in the position of Val82. Together, these observations suggest that in the 26S, ATPases' C termini bind into specific intersubunit pockets in the α ring, and that occupancy of only one or a few key pockets is sufficient to cause the rotation of specific α subunits that trigger gate opening for substrate entry.

EXPERIMENTAL PROCEDURES

Protein and Peptides

The *T. acidophilum* 20S was prepared as previously described (Zwickl et al., 1999). All 20S mutants were generated by overlapping PCR site-directed mutagenesis. All peptides were synthesized by EZBiolab (Westfield, IN) and were purified by HPLC to 95%–99% purity (Smith et al., 2007). Gate opening of the wild-type and mutant *T. acidophilum* 20S was measured by following the established protocol (Smith et al., 2007).

Cryo-EM and Image Processing

To saturate binding sites in the 20S, all peptides were used at a high concentration (1 mM) and were incubated with the 20S for at least 10 min at 20°C. A drop of 2.5 μl of the sample mixture was applied to glow-discharged Quantifoil holey carbon grids (Quantifoil, Micro Tools GmbH, Germany), blotted with filter paper, and plunged into liquid ethane using a Vitrobot (FEI Company, USA). Grids of frozen hydrated samples were imaged using a Tecnai F20 electron microscope equipped with a field-emission gun (FEI Company, USA) and operated at an acceleration voltage of 200 kV. Micrographs at a defocus ranging from −1.5 to −3.5 μm were recorded at a nominal resolution of 50,000× on Kodak SO-163 films following strict low-dose procedures. The films were developed for 12 min with full-strength Kodak D-19 developer at 20°C. Figure S1A is a typical image of 20S embedded in vitreous ice, defocused −3.5 μm.

Micrographs free of drift were digitized with a Zeiss SCAI scanner using a step size of 7 μm. The digitized micrographs were binned over 2 × 2 pixels initially, with a calibrated pixel size of 2.74 Å on the specimen level. The program CTFFIND3 (Mindell and Grigorieff, 2003) was used to determine the defocus values for the micrographs. All particles (in both top and side views) were manually selected using Ximdisp, the display program associated with the MRC program suite (Crowther et al., 1996). More than 40,000 particles were selected from each sample, except the 20S-GTDHMVS, where only about 27,000 particles were used for the 3D reconstruction. Typically more than 90% of particles are in side views, which alone are sufficient to define the complete structures of the barrel-shaped 20S proteasome. FREALIGN (Grigorieff, 2007) was used for the refinement of Euler angles, in plan x-y shift of all particles, as well as for the contrast transfer function (CTF) correction and 3D reconstruction. A density map calculated from the atomic structure of *T. acidophilum* (PDB code, 1PMA) filtered to a resolution of 40 Å was used as initial model. D7 symmetry was applied in the 3D reconstructions. Any unoccupied binding sites in some of the particles, which are expected to be very few due to high concentration of peptides, will be averaged out and not visible in the final 3D reconstruction. Fourier shell correlation curves of all 3D reconstructions are shown in Figure S1B. The resolutions are the nominal resolutions based on the FSC = 0.143 criterion (Rosenthal and Henderson, 2003). When a 3D reconstruction reached a resolution better than 7.5 Å, images without binning (1.37 Å/pixel) were used for both refinement and 3D reconstruction by FREALIGN. The surface-rendered views of the density maps were produced with the program Chimera (Pettersen et al., 2004). The difference map was calculated by subtracting 20S from 20S-peptide complexes using the program diffmap.exe (provided by Nikolaus Grigorieff, Brandeis University), which normalizes the density maps before calculating the difference map. The 3D reconstructions were filtered to the resolution of 9 Å before calculating the difference map, to prevent differences caused by different resolutions. Three density maps with highest resolutions were low-pass filtered to the same resolution of 6.8 Å. A negative B factor of 700 $Å^2$ was applied to all the maps (in reciprocal space as $\exp[-0.25Bs^2]$, s is resolution in $Å^{-1}$). Docking of the atomic structures into the 3D density maps was refined by using rigid body refinement in MAVE in the RAVE package of Uppsala Software Factory (command IMPROVE) (Kleywegt et al., 2001).

We used the atomic structure of Arg10 to Ile12 from *A. fulgidus* (PDB code, 1J2Q [Groll et al., 2003]) to extend from Thr13 of *T. acidophilum* 20S (1PMA) and fit into the density of 20S with closed-gate conformation, using program O (Jones et al., 1991). We used the atomic structure of Ala7 to Ile12 from 20S-PA26 complex (1YA7 [Forster et al., 2005]) to extend from Thr13 of *T. acidophilum* 20S (1PMA) and fit into the density of 20S-AHLDVLYA complex with an open-gate conformation. We used only rigid body movement to describe the conformational change of the α subunits, and most α helices in the α subunit fit well into the density map after this rigid body conformational change.

ACCESSION NUMBERS

The coordinates have been deposited in the Protein Data Bank under accession numbers 3C91 (open-gate conformation) and 3C92 (closed-gate conformation).

SUPPLEMENTAL DATA

Supplemental Data include one table and six figures and can be found with this article online at http://www.molecule.org/cgi/content/full/30/3/360/DC1/.

ACKNOWLEDGMENTS

We thank Thomas Walz and Daniel Finley for critical reading of the manuscript, and Mary Dethavong for valuable assistance. J.R. was supported by a scholarship from the German Academic Exchange Service (DAAD). D.M.S. was supported by a fellowship from The Medical Foundation. This study has been supported in part by a grant from the NIH (R01GM082893) and a grant from Sandler Family Supporting Foundation (Sandler Program in Basic Science) to Y.C. and by grants from the NIH (5 R01 GM51923-09) and Fund for Innovation from Elan, Inc. to A.L.G., who is a senior fellow of the Ellison Foundation. J.R. and Y.C. solved and interpreted structure; D.M.S. prepared the proteins and peptides, did biochemistry analysis of 20S mutant, and interpreted the data; Y.Y. did 20S mutations, prepared PA26 protein, and did negative-staining EM; S.-C.C. did 20S mutations; and D.M.S., A.L.G., and Y.C. interpreted the data and wrote the manuscript.

Received: January 8, 2008
Revised: February 16, 2008
Accepted: March 7, 2008
Published: May 8, 2008

REFERENCES

Benaroudj, N., and Goldberg, A.L. (2000). PAN, the proteasome-activating nucleotidase from archaebacteria, is a protein-unfolding molecular chaperone. Nat. Cell Biol. *2*, 833–839.

Benaroudj, N., Zwickl, P., Seemuller, E., Baumeister, W., and Goldberg, A.L. (2003). ATP hydrolysis by the proteasome regulatory complex PAN serves multiple functions in protein degradation. Mol. Cell *11*, 69–78.

Coux, O., Tanaka, K., and Goldberg, A.L. (1996). Structure and functions of the 20S and 26S proteasomes. Annu. Rev. Biochem. *65*, 801–847.

Crowther, R.A., Henderson, R., and Smith, J.M. (1996). MRC image processing programs. J. Struct. Biol. *116*, 9–16.

DeLaBarre, B., and Brunger, A.T. (2005). Nucleotide dependent motion and mechanism of action of p97/VCP. J. Mol. Biol. *347*, 437–452.

Dubiel, W., Pratt, G., Ferrell, K., and Rechsteiner, M. (1992). Purification of an 11 S regulator of the multicatalytic protease. J. Biol. Chem. *267*, 22369–22377.

Forster, A., Whitby, F.G., and Hill, C.P. (2003). The pore of activated 20S proteasomes has an ordered 7-fold symmetric conformation. EMBO J. *22*, 4356–4364.

Forster, A., Masters, E.I., Whitby, F.G., Robinson, H., and Hill, C.P. (2005). The 1.9 Å structure of a proteasome-11S activator complex and implications for proteasome-PAN/PA700 interactions. Mol. Cell *18*, 589–599.

Goldberg, A.L. (2005). Nobel committee tags ubiquitin for distinction. Neuron *45*, 339–344.

Grigorieff, N. (2007). FREALIGN: High-resolution refinement of single particle structures. J. Struct. Biol. *157*, 117–125.

Groll, M., Ditzel, L., Lowe, J., Stock, D., Bochtler, M., Bartunik, H.D., and Huber, R. (1997). Structure of 20S proteasome from yeast at 2.4 Å resolution. Nature *386*, 463–471.

Groll, M., Bajorek, M., Kohler, A., Moroder, L., Rubin, D.M., Huber, R., Glickman, M.H., and Finley, D. (2000). A gated channel into the proteasome core particle. Nat. Struct. Biol. *7*, 1062–1067.

Groll, M., Brandstetter, H., Bartunik, H., Bourenkow, G., and Huber, R. (2003). Investigations on the maturation and regulation of archaebacterial proteasomes. J. Mol. Biol. *327*, 75–83.

Jones, T.A., Zou, J.Y., Cowan, S.W., and Kjeldgaard, M. (1991). Improved methods for building protein models in electron density maps and the location of errors in these models. Acta Crystallogr. A *47*, 110–119.

Kleywegt, G.J., Zou, J.-Y., Kjeldgaard, M., and Jones, T.A. (2001). Around O. In International Tables for Crystallography. Volume F. Crystallography of Biological Macromolecules, M.G. Rossmann and E. Arnold, eds. (Dordrecht, The Netherlands: Kluwer Academic Publishers), pp. 353–356.

Knowlton, J.R., Johnston, S.C., Whitby, F.G., Realini, C., Zhang, Z., Rechsteiner, M., and Hill, C.P. (1997). Structure of the proteasome activator REGalpha (PA28alpha). Nature *390*, 639–643.

Kohler, A., Cascio, P., Leggett, D.S., Woo, K.M., Goldberg, A.L., and Finley, D. (2001). The axial channel of the proteasome core particle is gated by the Rpt2 ATPase and controls both substrate entry and product release. Mol. Cell *7*, 1143–1152.

Lowe, J., Stock, D., Jap, B., Zwickl, P., Baumeister, W., and Huber, R. (1995). Crystal structure of the 20S proteasome from the archaeon T. acidophilum at 3.4 Å resolution. Science *268*, 533–539.

Ma, C.P., Slaughter, C.A., and DeMartino, G.N. (1992). Identification, purification, and characterization of a protein activator (PA28) of the 20 S proteasome (macropain). J. Biol. Chem. *267*, 10515–10523.

Masson, P., Andersson, O., Petersen, U.M., and Young, P. (2001). Identification and characterization of a Drosophila nuclear proteasome regulator. A homolog of human 11 S REGgamma (PA28gamma). J. Biol. Chem. *276*, 1383–1390.

Mindell, J.A., and Grigorieff, N. (2003). Accurate determination of local defocus and specimen tilt in electron microscopy. J. Struct. Biol. *142*, 334–347.

Pettersen, E.F., Goddard, T.D., Huang, C.C., Couch, G.S., Greenblatt, D.M., Meng, E.C., and Ferrin, T.E. (2004). UCSF Chimera—a visualization system for exploratory research and analysis. J. Comput. Chem. *25*, 1605–1612.

Rosenthal, P.B., and Henderson, R. (2003). Optimal determination of particle orientation, absolute hand, and contrast loss in single-particle electron cryomicroscopy. J. Mol. Biol. *333*, 721–745.

Seemuller, E., Lupas, A., Stock, D., Lowe, J., Huber, R., and Baumeister, W. (1995). Proteasome from Thermoplasma acidophilum: a threonine protease. Science *268*, 579–582.

Seong, I.S., Kang, M.S., Choi, M.K., Lee, J.W., Koh, O.J., Wang, J., Eom, S.H., and Chung, C.H. (2002). The C-terminal tails of HslU ATPase act as a molecular switch for activation of HslV peptidase. J. Biol. Chem. *277*, 25976–25982.

Smith, D.M., Kafri, G., Cheng, Y., Ng, D., Walz, T., and Goldberg, A.L. (2005). ATP binding to PAN or the 26S ATPases causes association with the 20S proteasome, gate opening, and translocation of unfolded proteins. Mol. Cell *20*, 687–698.

Smith, D.M., Chang, S.C., Park, S., Finley, D., Cheng, Y., and Goldberg, A.L. (2007). Docking of the proteasomal ATPases' carboxyl termini in the 20S proteasome's alpha ring opens the gate for substrate entry. Mol. Cell *27*, 731–744.

Voges, D., Zwickl, P., and Baumeister, W. (1999). The 26S proteasome: a molecular machine designed for controlled proteolysis. Annu. Rev. Biochem. *68*, 1015–1068.

Whitby, F.G., Masters, E.I., Kramer, L., Knowlton, J.R., Yao, Y., Wang, C.C., and Hill, C.P. (2000). Structural basis for the activation of 20S proteasomes by 11S regulators. Nature *408*, 115–120.

Zhang, Z., Clawson, A., Realini, C., Jensen, C.C., Knowlton, J.R., Hill, C.P., and Rechsteiner, M. (1998). Identification of an activation region in the proteasome activator REGalpha. Proc. Natl. Acad. Sci. USA *95*, 2807–2811.

Zwickl, P., Ng, D., Woo, K.M., Klenk, H.P., and Goldberg, A.L. (1999). An archaebacterial ATPase, homologous to ATPases in the eukaryotic 26 S proteasome, activates protein breakdown by 20 S proteasomes. J. Biol. Chem. *274*, 26008–26014.